Micro Pulse Lidar as a Tool for Active Remote Sensing of Atmospheric Particulate

B.Sudharshan Reddy[#1], Y.Bhavani Kumar [*2]
[#] RGUKT-IIIT, R. K.Valley-516329, Vempalli Mandal, Kadapa (Dist), AP, India
[1] sudharshan115@gmail.com

[*] National Atmospheric Research Laboratory, Department of Space, Government of India,
Gadanki-517112, Pakala Mandal, Chittoor (Dist), AP, India
[2] ypbk@narl.gov.in

Abstract— **Lidars have been employed in the investigation of instantaneous vertical structure of atmospheric particulate. Remote measurements of particle backscattering and aerosol extinction coefficient provide the altitude distribution of particles existence in the atmosphere. This paper describes the technology of micro pulse lidar employed for computation of altitude profiles of particle backscattering and extinction coefficient. The vertical distribution of particles in the atmosphere was derived using a code developed in MATLAB. Enhancement of particle vertical distribution during the period of 2007 Diwali was shown as a case study.**

Keyword-Remote sensing, micro pulse lidar, atmospheric particulate, Inversion mathematics, backscattering coefficient, extinction coefficient

I. INTRODUCTION

Remote sensing is a specialized field of measurement. In this technique, measurement of a parameter under test is done with no physical contact. Active remote sensing utilizes a dynamic source to interact with a target of interest and sense the attitude of target. Several active remote sensing techniques have been developed making use of radio, optical, and acoustic sources. The advantage of active remote sensing is that it provides range resolved measurement of parameter under investigation. Remote sensing methods making use of radio signals have been employed for characterization of target movement, location, rotation, and position [1, 2]. Acoustic methods of remote sensing have been used for measurement of mixing height and temperatures [3, 4].

Lidars work on the principle of radar [5]. In general, lidar systems employ lasers for probing the targets. Laser frequencies fall between infrared (IR) and ultraviolet (UV) band of electromagnetic (EM) spectrum. Lasers generate photons (packets of energy) and propagate them in the direction of beam focussed. Targets in the beam path scatter photons. Since lidar frequencies are much smaller compared to radio spectrum, the basic constituents such as particles known as particulate matter (PM), pollutants, gas molecules, agricultural residue, biological aerosol, atoms, etc,. act as targets at light wavelengths and produce echo returns. The lidar signals constitute backscattered photons in range resolved fashion. The range resolved backscattered photons are processed to extract target information such as range, strength and type of target [6, 7, and 8]. Lidars have applications in satellite laser ranging (SLR), topography, vegetation, mining, surveillance, archaeology, traffic control, pollution, and climate change.

In the recent years, the environment is disturbed by the advancement in human activities. Contamination to air, water and ecology domains cause peril to the environment. Routine human works such as agriculture, industrial, transport, construction, mining, bore-well rigging, and deforestation generate a large amount of atmospheric particulate (AP). These particles originate with different sizes and are well mixed with the atmosphere due to local winds. Sometimes the atmosphere is polluted heavily due to specific events like New Year eve, Diwali festival, and air shows etc. Firecrackers burnt during these events inject the additional amount of AP in to the atmosphere. The burnings of firecracker generate toxic elements like sulphur dioxide, potassium, nitrite, carbon, magnesium, cadmium, carbon dioxide, carbon monoxide. These elements get mixed with the atmosphere quickly and transported by the local wind. The increase of total particle load in the atmosphere is difficult to access because of distributive nature of particles. Particles smaller than 2.5 micron suspend in the atmosphere for longer periods and contribute significantly to the air quality of the atmosphere. Shorter and long term effects of environment depend on the presence of fine particles in the atmosphere. Fine particles generated by the anthropogenic sources affect human health severely and cause some epidemic diseases [9, 10, 11, 12, and 13]. Real-time assessment of particle load in the atmosphere is difficult due to lack of availability of advanced technology. Active laser remote sensing of atmosphere provides the instantaneous information on the particle distribution and their temporal variability. Laser sources are producers of artificial light with monochromatic spectrum at narrow beam divergences. Photons generated by lasers interact with the basic constituents of the atmosphere and undergo scattering phenomenon. Particles interaction with light is governed by Mie scattering [14], where as interaction of gas molecules with light is explained using Rayleigh scattering [15].

II. MICRO PULSE LIDAR

Lidars operate on different techniques. The lidar system used in this study operates on the principle of micro pulsing [16]. The lidar system described here was developed at National Atmospheric Research Laboratory (NARL), a Department of Space and Government of India unit located at a rural site named Gadanki (13.5°N,79.2°E, 375m AMSL) in Chittoor district of Andhra Pradesh state in India. The lidar system was developed for ranging the atmospheric boundary layer (ABL) and was described in detail elsewhere [17]. In this method, the employed laser produces high frequency light pulses at energies in the range of micro joules. The high frequency low pulse energy lasers generation is possible only with diode pumped mechanism. Diode pumped solid state lasers (DPSS) are semiconductor lasers produce fine laser beams with narrow pulse widths which are not possible with conventional type lasers. DPSS lasers have several advantages over conventional types such as good spectral purity, continuous performance, no audible sound during work, miniature structure, long-life and low cost. Lidars using micro pulse method employ transmitter optics like beam expander, photon collecting optics such as telescope, photo detector for converting photons into electrical pulses and data processing electronics similar to conventional systems. Figure 1 shows the schematic block diagram of the micro pulse lidar developed at NARL site, Gadanki.

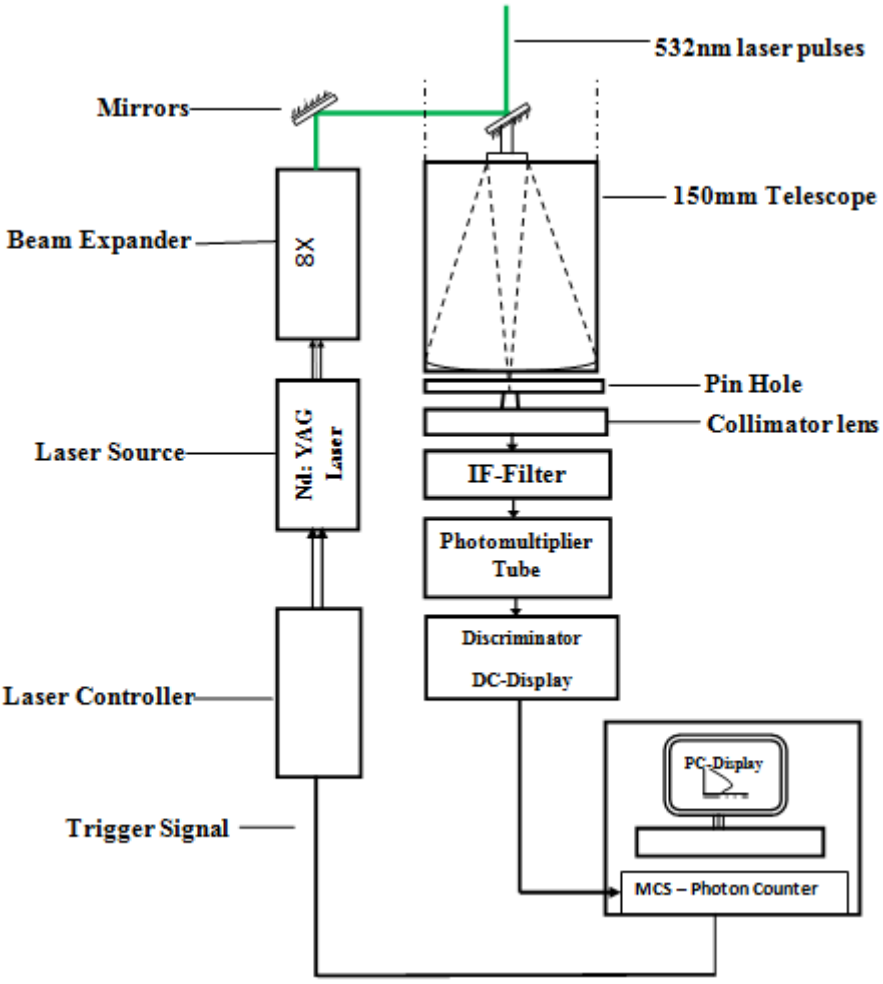

Fig. 1 Schematic of micro pulse lidar system employed in this study

The technology of NARL micro pulse lidar is given in the following lines. The lidar system employs (a) DPSS Laser (b) Light collecting optics (c) Detector unit (d) Data acquisition system.

(a) DPSS laser: The NARL micro pulse lidar uses a single microchip YAG crystal pumped by diode lasers. The laser delivers second harmonic of Nd:YAG, which is 532 nm in wavelength. The laser employed was Laser export, Russian make system. The laser system was employed with an acoustic switching unit for generating variable inter-pulse period in laser output. The laser pulse energy can be settable between 2 and 20 μJ depending on the repetition rate. Usually the laser was set at 10 micro joules with a pulse repetition rate of 2500. Fine beam of polarized laser exits the laser unit.

(b) Light collecting optics: A classical Cassegrain telescope unit was employed as the light collecting optics unit. The reflecting optics diameter of telescope was 150 mm. The focal ratio was 9. The telescope was arranged over a sturdy structure with a provision to tilt and rotate.

(c) Detector: A high gain photomultiplier tube (PMT) was employed as the detector unit for converting the photons to electrical signals. The PMT operation requires a high voltage DC supply for biasing purpose. The gain of the PMT depends on the DC voltage regulation.

(d) Data acquisition system: Photon counter was employed in this lidar for generating the range resolved photon count data from PMT signals. The photon counter used was a high density and multi-layer PCB card. The photon counting system was used as a add-on card to a personal computer for generating the photon count profile. The card works on the principle of time of flight measurement.

In the NARL lidar system, an external beam expander was used to collimate the outgoing laser beam. The lidar transmit-receive system was designed with coaxial configuration. Two high reflecting mirrors were used to divert the laser beam on to the receiver axis to achieve this configuration. A conventional cassegrain telescope was employed for collecting the laser backscattered photon returns. A pin hole with 0.5 mm diameter was used as the IRIS. A narrow interference filter (IF) with one inch diameter was employed to differentiate the collected photon spectrum from the background. A pulse discriminator was employed as the buffer to drive the PMT output pulses to photon counter. The laser control unit triggers the photon counter for every pulse of laser transmission.

III. LIDAR SIGNAL DESCRIPTION AND PROCESSING

The lidar is a compact system that can be operated by a single person. The system can be oriented at any elevation angle, however, generally operated in the zenith direction. The altitude profiles of photon count data from the NARL lidar system generally cover the upper troposphere region during clear sky night periods. The photon count data collected by the lidar is governed by many factors like laser energy per pulse, wavelength of operation, atmospheric transmission at laser wavelength, collecting area of the receiver, and efficiencies of transmitter and receiver optics [18]. The lidar system output performance is explained by means of an expression shown in Equation-1, which is popularly known as lidar equation [19].

$$P(z) = E_S A \frac{O(z)}{z^2} \beta_T(z) \eta_L T^2(z) + P_b \qquad \text{-- (1)}$$

Various terms used in the above equation are explained in the following lines.

$P(z)$ = Lidar signal intensity in photons

z = Range

E_S = Energy of transmitted photons at the wavelength of laser

η_L = Lidar system Efficiency

$O(z)$ = Overlap Function

$T(z)$ = Transmission of the atmosphere

$\beta_T(z)$ = Total backscattering Coefficient of targets = $\beta_m(z) + \beta_p(z)$

A = Receiving telescope collecting area

$\beta_m(z)$ = Molecular Backscattering Coefficient

$\beta_p(z)$ = Particle Backscattering coefficient

$\alpha_p(z)$ = particle extinction coefficient

$\alpha_m(z)$ = Molecular extinction coefficient

P_b = Total noise generated by the sources from external and internal to the lidar

The lidar system is usually operated during nocturnal periods at lidar site. The method of signal acquisition employed was photon counting. Generally, the lidar was operated at one or two minute time integration with 30m vertical resolution (range gate). An integration of 150000 laser shots constitutes a meaningful photon count profile. This forms the raw data signal. It corresponds to a time span of 60 sec. A lidar signal integrated over 300 sec time span is shown in Figure 2. The lidar data presented in Figure 2 was collected on the day of November 07, 2007. Three panels correspond to lidar data were shown in form of an image in Figure 2. Panel (a) of Figure 2 indicates the raw data signal from lidar, which presents the altitude distribution of accumulated photon counts collected between 2345 and 2350 LT on the observational day at the lidar site. Panel (b) of Figure 2 represents background corrected photon count profile. This picture is generated from the panel (a) of Figure 2. Usually lidar background P_b is estimated from the photon counts received at heights above 30000m. The estimated mean background is removed from the measured photon counts received at each range gate.

The background corrected form of lidar signal is expressed mathematically as $[P(z) - P_b]$. – (2)

Then the range correction is considered to compensate for the signal path loss. The path loss was due to scattering of photons during laser traverse in the atmosphere. The mathematical formula showing the path loss correction to the noise corrected photon count data is given by Equation (3). The panel (c) of Figure 2 illustrates the range correction to noise corrected signal shown in panel (b) of Figure 2.

$$X(z) = [P(z) - P_b]z^2 \qquad \text{-- (3)}$$

A peak at 14 km altitude shown in all panels of Figure 2 indicates the detection of high altitude cloud layer. Clouds produce strong scattering to laser beam because they composed of large number of hydrometeor. A strong layer of signal at altitude between 150 and 3000 m in panel (c) of Figure 2 indicates the local boundary layer containing a large amount of AP. The range corrected photon count data shown in panel (c) of Figure 2 is used in the inversion mathematics for obtaining the optical characteristics of particles.

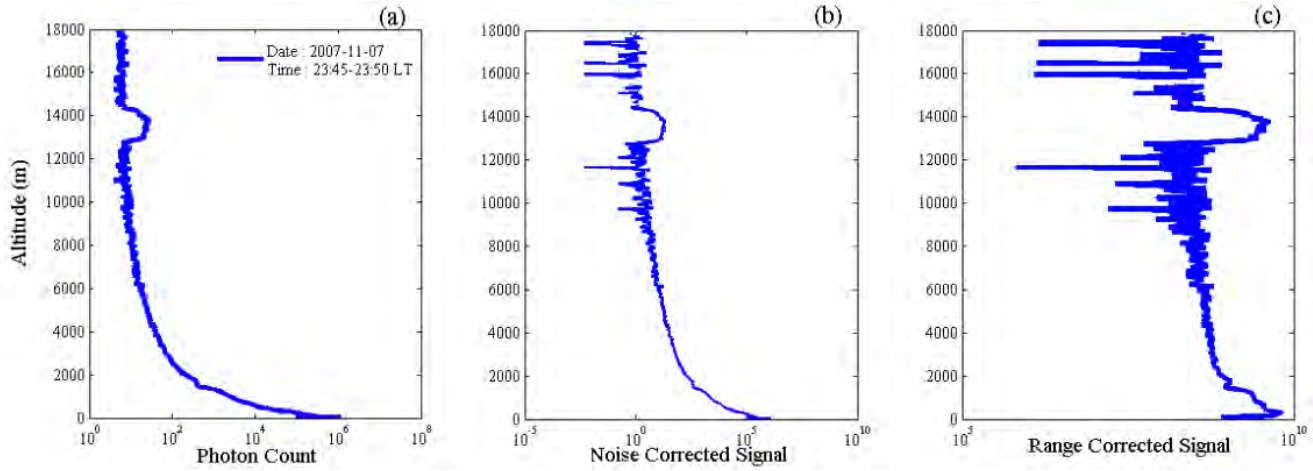

Fig. 2 Altitude distributions of photon count data collected using lidar system. The data shown was obtained on 7 November 2007 during the period between 2345 and 2350 LT. Panel (a) represents the raw data of lidar, Panel (b) shown altitude distribution of photon count data corrected for background and the panel(c) indicates range corrected photon count data. A strong layer of signal shown at ranges between 13 and 15 represent lidar detection of high altitude cloud layer

IV. LIDAR SIGNAL INVERSION

Laser light interactions with particles and molecules define the amount of backscattering and transmission loss to the laser propagation in the atmosphere. Atmospheric particles encountered in the path of laser beam undergo Mie scattering and the air molecules suffer from Rayleigh scattering. Since the contributions are different, it needs to be considered separately. Equations 4 and 5 narrate the explanation mathematically,

$$\beta_T(z) = \beta_m(z) + \beta_p(z) \qquad \text{-- (4)}$$

$$T^2(z) = \exp\left[-2\int_0^z \alpha_T(z).dz\right] \qquad \text{-- (5)}$$

$$\text{Where} \quad \alpha_T(z) = \alpha_m(z) + \alpha_p(z)$$

Using above combinations, the range corrected lidar signal can be expressed as

$$X(z) = [P(z) - P_b]z^2 = E_s A \eta_L \left[\beta_m(z) + \beta_p(z)\right].\exp\left[-2\int_0^z \{\alpha_m(z) + \alpha_p(z)\}.dz\right] \qquad \text{-- (6)}$$

To further simplify the above equation, a relationship between backscattering and extinction coefficient is assumed. The new parameter known as lidar ratio can be defined for particles and molecules as shown. Lidar ratio is constant if there is no variability in the target cross-section for a fixed wavelength of probing. This is true in the case of molecules; however, the particles have size distribution and can contribute to variable lidar ratio with altitude [20].

$$L_p(z) = \frac{\alpha_p(z)}{\beta_p(z)} \qquad \text{-- (7)}$$

$$L_m = \frac{\alpha_m(z)}{\beta_m(z)} = \frac{8\pi}{3}\ \text{sr} \qquad \text{-- (8)}$$

Then the equation (6) becomes,

$$X(z) = E_s A \eta_L \left[\beta_m(z) + \beta_p(z)\right].\exp\left[-2\int_0^z \{L_m\beta_m(z) + L_p(z)\beta_p(z)\}.dz\right] \qquad \text{-- (9)}$$

Defining a new parameter Y(z), we get

$$Y(z) = L_p(z)\left[\beta_m(z) + \beta_p(z)\right] \qquad \text{-- (10)}$$

Then equation (9) becomes ,

$$X(z) = E_s A \eta_L \frac{Y(z)}{L_p(z)} . \exp\left[-2 \int_0^z \{Y(z) - \beta_m(z)\left[L_p(z) - L_m\right]\} . dz\right] \quad \text{-- (11)}$$

$$X(z) . L_p(z) . \exp\left[-2 \int_0^z \beta_m(z)[L_p(z) - L_m] . dz\right] = E_s A \eta_L Y(z) . \exp\left[-2 \int_0^z Y(z) . dz\right] \quad \text{-- (12)}$$

Applying natural logarithm and derivative to simplify the Equation (12) further, we get

$$\frac{d\{\ln\{X(z).L_p(z).\exp\left[-2 \int_0^z \beta_m(z)[L_p(z)-L_m].dz\right]\}\}}{dz} = \frac{d\{\ln[E_s A \eta_L] + \ln Y(z) - 2 \int_0^z Y(z).dz\}}{dz} \quad \text{-- (13)}$$

Defining a new variable T as shown in Equation – (14)

$$T = \ln X(z) . L_p(z) . \exp\left[-2 \int_0^z \beta_m(z)[L_p(z) - L_m] . dz\right] \quad \text{-- (14)}$$

Then equation (13) becomes,

$$\frac{d}{dz}(T) = \frac{1}{Y(z)} . \frac{dY(z)}{dz} - 2Y(z) \quad \text{-- (15)}$$

Further simplifying, we get

$$Y(z) . \frac{d}{dz}(T) = \frac{dY(z)}{dz} - 2Y^2(z) \quad \text{-- (16)}$$

It is first order differential equation of Bernoulli form. Solving the equation (16) gives

$$\frac{1}{Y(z)} . X(z) . L_p(z) . \exp\left[-2 \int_0^z \beta_m(z)[L_p(z) - L_m] . dz\right] =$$

$$-2 \int_0^z X(z) . L_p(z) . \exp\left[-2 \int_0^z \beta_m(z)[L_p(z) - L_m] . dz\right] . dz + C \quad \text{-- (17)}$$

Substitute Y (z) in Eq (17), we get

$$\frac{1}{L_p(z)\left[\beta_m(z) + \beta_p(z)\right]} . X(z) . L_p(z) . \exp\left[-2 \int_0^z \beta_m(z)[L_p(z) - L_m] . dz\right]$$

$$= -2 \int_0^z X(z) . L_p(z) \exp\left[-2 \int_0^z \beta_m(z)[L_p(z) - L_m] . dz\right] . dz + C$$

After rearranging the terms, we get

$$\left[\beta_m(z) + \beta_p(z)\right] = \frac{X(z).\exp\left[-2 \int_0^z \beta_m(z)[L_p(z)-L_m].dz\right]}{C - 2 \int_0^z X(z).L_p(z)\exp\left[-2 \int_0^z \beta_m(z)[L_p(z)-L_m].dz\right].dz} \quad \text{-- (18)}$$

The Equation (18) gives the total backscattering produced by air molecules and particles in the probed target volume. If boundary condition is known, we can calculate the value of C in the above equation. In order to compute C, we assume a distant range, zo, from the lidar where the particle presence is negligible or very small compared to the molecular concentration. If so, at z_0, the signal counts received at the lidar are mainly contributed by only air molecules. By applying the boundary condition to the equation (18), we obtain the C value as $\frac{X(z_0)}{\beta_t(z_0)}$.

Then the total backscattering coefficient is given as the equation (19),

$$\beta_T(z) = \left[\beta_m(z) + \beta_p(z)\right] = \frac{X(z).\exp\left[-2 \int_0^z \beta_m(z)[L_p(z)-L_m].dz\right]}{\frac{X(z_0)}{\beta_t(z_0)} - 2 \int_0^z X(z).L_p(z)\exp\left[-2 \int_0^z \beta_m(z)[L_p(z)-L_m].dz\right].dz} \quad \text{-- (19)}$$

The particle backscattering coefficient can be computed by simply subtracting the altitude dependent molecular backscattering from the total backscatter. This gives the altitude distribution of particle backscattering coefficient as shown in equation (20)

$$\beta_p(z) = -\beta_m(z) + \frac{X(z).\exp\left[-2 \int_0^z \beta_m(z)[L_p(z)-L_m].dz\right]}{\frac{X(z_0)}{\beta_t(z_0)} - 2 \int_0^z X(z).L_p(z)\exp\left[-2 \int_0^z \beta_m(z)[L_p(z)-L_m].dz\right].dz} \quad \text{---- (20)}$$

This inversion procedure is known as Klett [21] method and the forward mode of solution is in Equation [20]. This solution requires reference calibration height and particle extinction-to-backscatter ratio $L_p(z)$ as priory. It may be noted that the solution shown in Equation (20) could become unstable for cases of high extinction and would diverge with increased height [21]. Hence, a "backward" solution is usually preferred. In this backward solution approach, a known calibration position was chosen beyond the region where the retrieval is to be performed. To facilitate this, reordering of the orders of integration and the change of sign in the denominator

are required in equation (20). This makes the solution more stable, provided the particle scattering coefficient in the calibration point can be estimated properly. The computation of particle extinction coefficient is usually made by multiplying the backscattering coefficient with lidar ratio and is given as

$$\alpha_p(z) = L_p(z).\beta_p(z)$$

Molecular extinction to backscattering ratio, described by L_m, is constant and is given as = 8pi/3 = 8.38. The particle extinction to backscattering ratio, $L_p(z)$ depends on the refractive index and particle size distribution. Its value varies from 10 to 100 depending upon the size, composition and refractive index of the particle. The molecular backscattering coefficient can be computed if the backscattering cross section σ_π of air molecules at the probing wavelength is known. Equation (21) provides the altitude dependent molecular backscattering coefficient.

$$\beta_m(z) = \frac{9\pi^2(n_{air}^2-1)^2(6+3\gamma)}{\lambda^4 N_s^2(n_{air}^2+2)^2(6-7\gamma)}(N_s)\frac{T_0}{P_0}\frac{P(z)}{T(z)} \qquad \text{-- (21)}$$

The term N_s indicates the molecular number density. It is derived using the local air temperature and pressure data. The other terms such as n_{air} represents the refractive index and γ indicates the depolarization of the air [16]. For standard atmospheric pressure (P_0= 1013.25mbar) and temperature (T_0 = 288.15K), the molecular number density is determined as $N_s = 2.547 \times 10^{25} m^{-3}$.

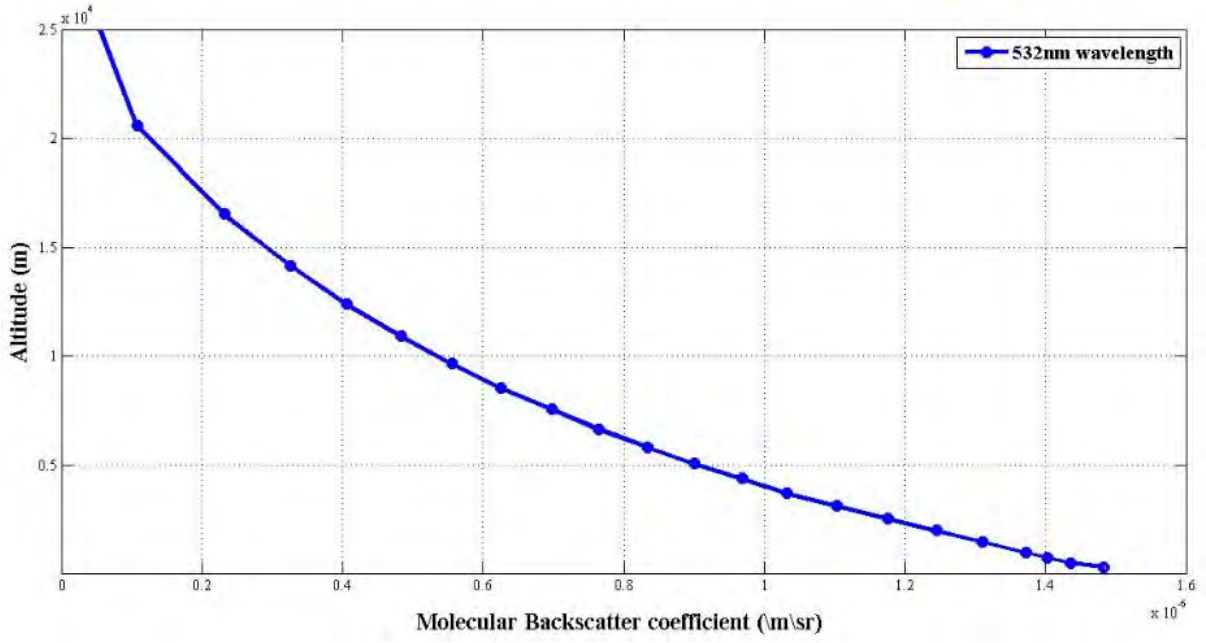

Fig. 3 Altitude distribution of molecular backscattering coefficient for probing wavelength of 532 nm

The altitude profile of molecular number density was calculated using the above equation employing the vertical profiles of temperature and pressure data obtained from NOAA READY site (http://www.ready.noaa.gov/). The NOAA READY site data collected in this connection was correspond to the coordinates of NARL site, Gadanki (13.5^{0}N, 79.2^{0}E, 375 m MSL), where the lidar was operated for conducting atmospheric investigations. The altitude profile of molecular backscattering coefficient derived for 532 nm wavelength is shown in Figure 3.

V. IMPLEMENTATION OF INVERSION MATHEMATICS

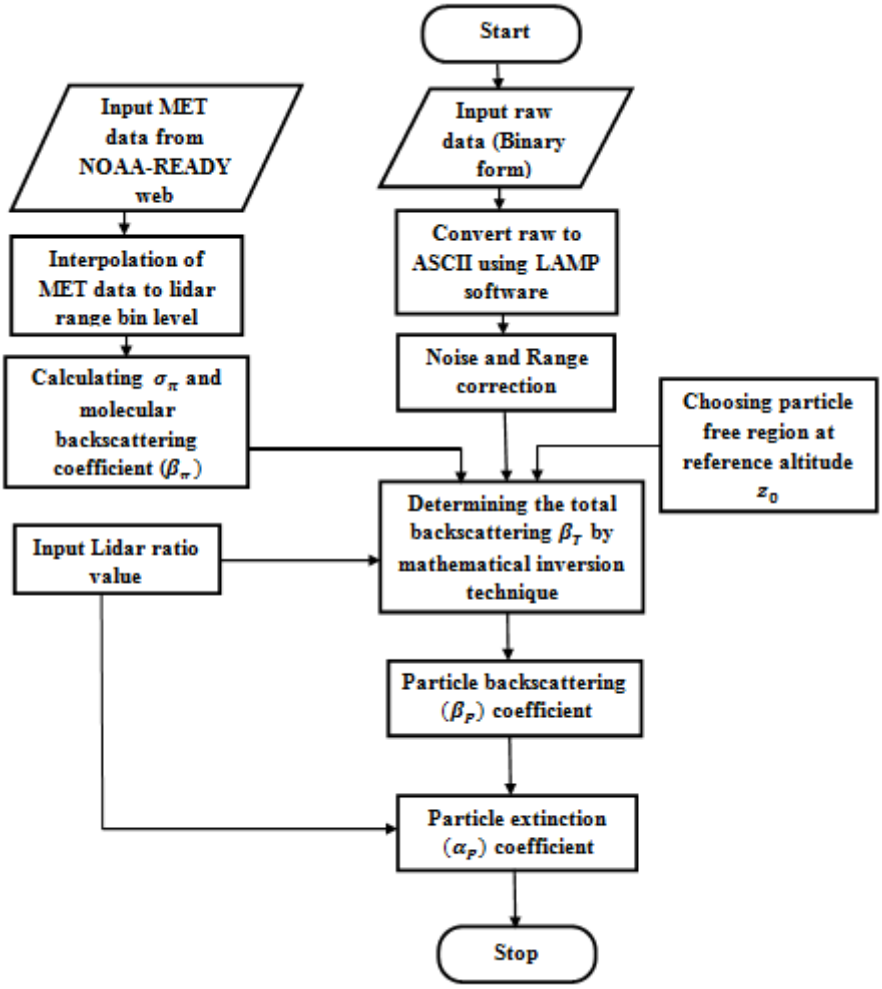

Fig. 4 Flow chart showing the algorithm employed in the MATLAB code developed for performing the inversion of lidar signals

The inversion of lidar signals was implemented in the MATLAB. The algorithm employing the MATLAB code was explained in the flow chart shown in Figure 4. The MATLAB code is available in the report of Mr B.Sudharashan Reddy, submitted to INSA-SRFP-2013. The MATLAB code was applied to lidar signals for deriving the atmospheric particulate backscattering and extinction coefficient. The total backscattering coefficient derived from lidar signals has been shown in Figure 5. Figure 5 illustrates the height profile of total backscattering coefficient presented up to an altitude of 18km. The green colored trace shown in Figure 5 indicates the molecular trace. The lidar data collected between 22:00 and 23:00 LT duration on November 07, 2007 were used for computation of altitude profile of total backscattering coefficient.

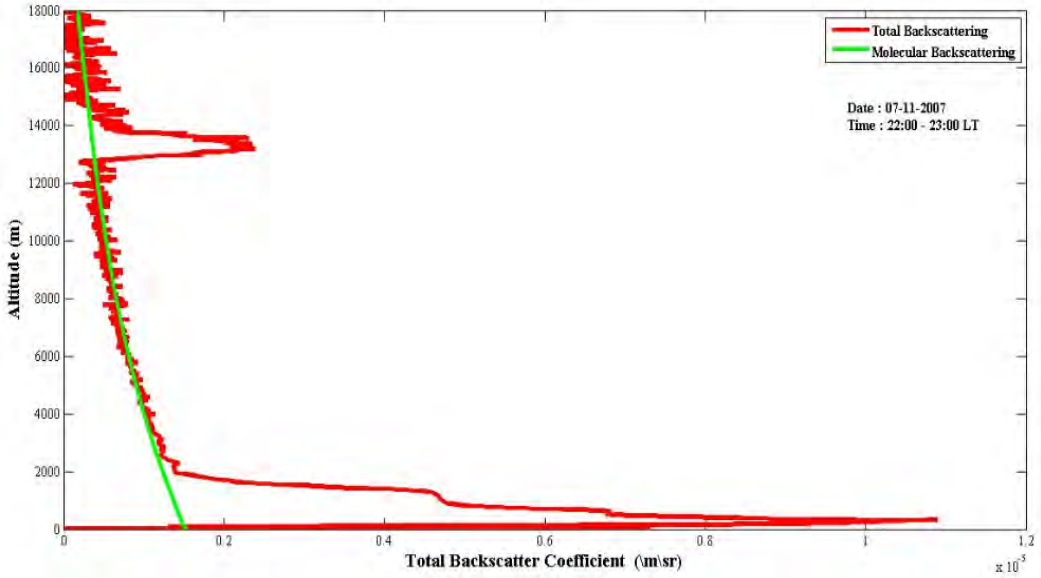

Fig. 5 Altitude profile of total backscattering coefficient derived from lidar signals. The lidar data shown was collected at lidar site on 07 November 2007 during the period between 22:00 and 23:00 LT.

VI. Results and Discussion

The indigenously developed micro pulse lidar at NARL site, Gadanki was used for remote measurements of particle distribution in the vertical scale. The lidar data presented in this study was collected during the period between 7 and 11 November 2007. On these days, the lidar operation was limited to a time period of six hours that is between 1900 and 0200 LT. During the investigation period, it was observed that 08 November 2007 was a cloudy day compared to other days. Only clear sky data was used in this study for discussion. The useful lidar data were subjected to inversion analysis. The averaged profiles of particle extinction coefficient computed from lidar data obtained on 07 and 09 November 2007 were presented in Figure 6. The color traces shown in red and blue represent the mean of two different nights. These days were selected to show the contribution of additional particle load into the atmosphere by an event occurred on the day of 08 November 2007. The red colored trace corresponds to the investigation day prior to event day, whereas the blue color trace shows the observation conducted after the event. Both observations show a large amount of extinction at lower heights of atmosphere. This is due to the presence of large amount of particles suspended in the local boundary layer. This layer is also known as the local dust layer.

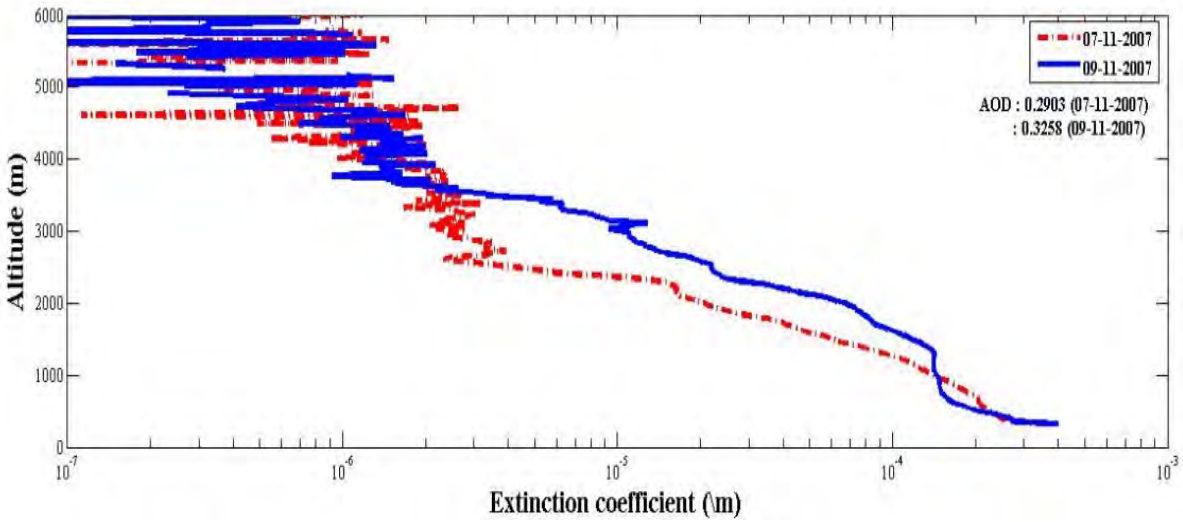

Fig. 6 Altitude profiles of atmospheric extinction computed using lidar measurements. Red colored trace corresponds to lidar data obtained on 07 November 2007, whereas blue colored trace represents 09 November 2007 lidar data

It may be seen that there is an increase in the particle extinction on 9 November 2007 compared to 07 November 2007 investigation. Additionally, the vertical extent of particle extinction was also high compared to 07 November 2007 observation. The lidar data were, later, subjected to particle load analysis by integrating the

extinction within the particle layer of lower atmosphere. The computed particle optical depth was appeared to be more on 09 November 2007 than 07 November 2007 case. The additional extinction on 09 November 2007 may be due to additional particles injected or transported in to the local dust layer. The background trajectory analysis using NOAA ready data (not shown) indicates that there is a transport from nearby civilian areas. The additional particle load on 09 November was due to contribution of PM on Diwali day, which was on 8 November 2007. During this day, the fire crackers are burnt in India on the eve of the holy festival [22]. Burnings of Firecrackers inject elements like sulphur dioxide, potassium, nitrite, carbon, magnesium, cadmium, carbon dioxide, carbon monoxide in to the boundary layer. The burnings of fire crackers release large amount fine metal and toxic PM in to the atmosphere, which in turn increase the particle load of the atmosphere [23, 24, 25, 26, and 27]. The analysis of lidar data on these days indicates that lidar is a potential instrument to detect the real-time particle load in the atmosphere.

VII. Conclusions

An application of lidar remote sensing of particle load in the atmosphere was explained in this paper. The lidar signals were subjected to inversion analysis to obtain the atmospheric particle backscattering and extinction coefficient profiles. The particle load was estimated using the integration of particle extinction that computed from the signals of lidar. The method of particle extinction estimation was explained from the first principles. The micro pulse lidar used in this study was developed at NARL, a Department of Space and Government of India laboratory. An observation of excess particle load in the atmosphere after the event of 2007 Diwali was compared with the lidar observations prior to the event. Lidar system is a potential ground based instrument for ascertaining the atmospheric particulate and particle layers in the atmosphere.

Acknowledgment

Authors would like to thank the authorities of NARL and the Atmospheric Science Programme (ASP) of Department of space for supporting the LIDAR project at NARL site, Gadanki. One of the authors, B.Sudharshan Reddy, would like to thank the Indian National Science Academy (INSA) for support of funding under the summer Research Fellowship programme (SRFP) -2013. He also would like to thank Prof.N. Mukunda, Indian Institute of Science (IISc), Bangalore for the support and help given under SRFP-2013.

References

[1] D. K. Barton, *Modern Radar System Analysis*, Artech House, Norwood, MA, 1988.
[2] E. Brookner, Editor, *Aspects of Modern Radar*, Artech House, Norwood, MA, 1988.
[3] F. Beyrich, *On the Use of Sodar Data to Estimate Mixing Height*, Appl. Phys. B 57, 27-35, 1993
[4] J. Kaimal, *Atmospheric Boundary Layer Flows*, Oxford University Press, United Kindom, 1994
[5] J. V. DiFranco, and W. L. Rubin, *Radar Detection*, Artech House, Norwood,MA, 1980.
[6] Y.Bhavani Kumar, C. Nageswara Raju and M. Krishnaiah, *Indo-Japanese Lidar Observations of the Tropical Middle Atmosphere during 1998 and 1999*, Advances in Atmospheric Sciences, 23 (5), 711-725, 2006.
[7] Y. Bhavani Kumar, D. N. Rao, M.Sundara Murthy and M. Krishnaiah, *Resonance lidar System for mesospheric sodium measurements*, Journal of Optical Engineering, 46, 086203, 2007.
[8] P. Rajitha, Y. Bhavani Kumar and T. Krishna Chaitanya, *Wavelet transform method for deriving atmospheric boundary layer height from lidar signals*, International Journal of Engineering and Technology, vol. 5, no. 2, 2013.
[9] B. Brunekreef, D. W. Dockery and M. Krzyzanowski, *Epidemiologic studies on short-term effects of low levels of major ambient air pollution components*, Environ Health Perspect, 103, 3-13,1995.
[10] H. Gong, P. A. Lachenbruch , P. Harber and W. S. Linn , *Comparative short-term helath responses to sulfur dioxide exposure and other common stresses in a panel of asthmatics*, Toxicol Ind Health, 11, 467-487, 1995.
[11] Peters , H. E. Wichmann , T. Tuch , J. Heinrich and J. Heyder , *Respiratory effects are associated with the number of ultrafine particles*, Am J Respir Crit Care Med, 155, 1376-1383,1997.
[12] K. Donaldson, D. Brown and A. Clouter, *The pulmonary toxicology of ultrafine particles*, J Aerosol Meds, 15, 213-220, 2002.
[13] D. Maynard and E. D. Kuempel, *Airborne nonstructured particles and occupational health*, J Nanoparticles Res, 7, 587-614, 2005.
[14] Gustav Mie, Beiträge zur Optik trüber Medien, speziell kolloidaler Metallösungen. Annalen der Physik, Vierte Folge, Band 25,No. 3, p 377-445,1908.
[15] John Strutt , *On the transmission of light through an atmosphere containing small particles in suspension, and on the origin of the blue of the sky*, Philosophical Magazine, series 5, vol. 47, pages 375-394,1899.
[16] J.D. Spinhirne, *Micro pulse lidar*, IEEE Trans. Geos.Rem. sen.31, 48-54, 1993.
[17] Y. Bhavani Kumar, *Portable lidar system for atmospheric boundary layer measurements*, Journal of Optical Engineering, 45, 076201, 2006.
[18] J.A. Reagan, M. P. McCormick, J. D. Spinhirne, *Lidar sensing of aerosols and clouds in the troposphere and stratosphere*. Proc. IEEE. **77**, pp. 433-448, 1989.
[19] R. T. H Collis: *Lidar for routine meteorological observations*, Bulletin of American Meteorological Society, 50 pp 688–694, 1969.
[20] A. Cattrall, J. Reagan, K. Thome, and O. Dubovik, *Variability of Aerosol and Spectral Lidar and Backscatter and Extinction Ratios of Key Aerosol Types Derived from Selected Aerosol Robotic Network Locations*. J. Geophys. Res. 110: D10S11, 2005.
[21] J. D. Klett, *Stable analytical inversion solution for processing lidar returns*, Applied Optics, 20, pp 211-220, 1981.
[22] U.C. Kulshrestha, T. Nageswara Rao , S. Azhaguvel and M. J. Kulshrestha , *Emissions and accumulation of metals in the atmosphere due to crackers and sparkles during Diwali festival in India*, Atmos Environ, 38, 4421-4425, 2004.
[23] Y. S. Balin, and I. A. Razenkov, *Laser Monitoring of Aerosol Pollution of Air Basin of Industrial Centers*, Atmos. Ocean. Opt., 6, p. 104-114, 1993.
[24] O. Boucher, and T. L. A. Anderson, *General circulation model assessment of the Sensitivity of direct climate forcing by anthropogenic sulfate aerosols to aerosol size and chemistry*. J. Geophys. Res., 100, 26117-26134, 1995.

[25] K. Ravindra, S. Mor & C.P. Kaushik, *Short-term variation in air quality associated with firework events: A case study*, J Environ Monit, **5**, 260-264, 2003.
[26] Y. Wang, G. Zhuang, C. Xu and Z. An, *The air pollution caused by the burning of fireworks during the lantern festival in Beijing*, Atmos Environ, 41, 417-431, 2007.
[27] R. Vecchi, V. Bernardoni, D. Cricchio, A. D'Alessandro, A. Fermo, F. Lucarelli, S. Nava, A. Piazzalunga and G. Valli, *The impact of fireworks on airborne particles*, Atmos Environ, 42, 1121-1132, 2008.